Separating the Indian and Pacific Ocean Impacts on the Euro-Atlantic Response to ENSO and Its Transition from Early to Late Winter

MUHAMMAD ADNAN ABID,[a,b] FRED KUCHARSKI,[a,b] FRANCO MOLTENI,[a,c], IN-SIK KANG,[d,e], ADRIAN M. TOMPKINS,[a] AND MANSOUR ALMAZROUI[b]

[a] *Earth System Physics, The Abdus Salam International Centre for Theoretical Physics, Trieste, Italy*
[b] *Centre of Excellence for Climate Change Research/Department of Meteorology, King Abdulaziz University, Jeddah, Saudi Arabia*
[c] *European Centre for Medium-Range Weather Forecasts, Reading, United Kingdom*
[d] *Indian Ocean Center, State Key Laboratory of Satellite Ocean Environment Dynamics, Second Institute of Oceanography, Ministry of Natural Resources, Hangzhou, China*
[e] *School of Oceanography, Shanghai Jiaotang University, Shanghai, China*

(Manuscript received 5 February 2020, in final form 1 November 2020)

ABSTRACT: The present study focuses on the mechanism that controls the transition of the Euro-Atlantic circulation responses to El Niño–Southern Oscillation (ENSO) from early (December) to late winter (February) for the period 1981–2015. A positive phase of ENSO induces a precipitation dipole with increased precipitation in the western and reduced precipitation in the eastern tropical Indian Ocean; this occurs mainly during early winter (December) and less so in late winter (February). It is shown that these interbasin atmospheric teleconnections dominate the response in the Euro-Atlantic sector in early winter by modifying the subtropical South Asian jet (SAJET) and forcing a wavenumber-3 response that projects spatially onto the positive North Atlantic Oscillation (NAO) pattern. On the contrary, during late winter, the response in the Euro-Atlantic sector is dominated by the well-known ENSO wave train from the tropical Pacific region, involving extratropical anomalies that project spatially on the positive phase of the Pacific–North American (PNA) pattern and the negative phase of the NAO pattern. Numerical experiments with an atmospheric model (an AGCM) forced by an Indian Ocean heating dipole anomaly support the hypothesis that the Indian Ocean modulates the SAJET and enforces the Rossby wave propagation to the Euro-Atlantic region in early winter. These phenomena are also investigated using the ECMWF SEAS5 reforecast dataset. In SEAS5, the ENSO interbasin tropical teleconnections and the response of the Euro-Atlantic circulation anomalies and their change from early to late winter are realistically predicted, although the strength of the early winter signal originated from the Indian Ocean is underestimated.

KEYWORDS: Indian Ocean; Atmosphere-ocean interaction; Dynamics; ENSO; Teleconnections; North Atlantic Oscillation

1. Introduction

El Niño–Southern Oscillation (ENSO) modulates the Euro-Atlantic atmospheric circulation during the boreal winter (December–February) season (e.g., Toniazzo and Scaife 2006; Brönnimann 2007; Bladé et al. 2008; García-Serrano et al. 2011; Jiménez-Esteve and Domeisen 2018; Domeisen et al. 2019; Trascasa-Castro et al. 2019; Hardiman et al. 2019; and others). The Euro-Atlantic circulation response to ENSO shows a transition from early to late winter through tropospheric (e.g., Moron and Gouirand 2003; Scaife et al. 2017; King et al. 2018a; Ayarzagüena et al. 2018; Mezzina et al. 2019) as well as through stratospheric pathways (e.g., Ineson and Scaife 2009; Sigmond et al. 2013; Domeisen et al. 2015; Ayarzagüena et al. 2019; and others), but our understanding of this response transition is still incomplete. In the current study, we are focusing on the role of forcing from heating anomalies in the tropical Indian Ocean and the central-eastern equatorial Pacific region to understand the early to late winter transition of the circulation anomalies over the Euro-Atlantic region by using observations and reanalysis as well as a seasonal hindcast dataset.

Several studies have investigated the Euro-Atlantic circulation responses to ENSO within the boreal winter season by separating the early and late part of the season in relation to the sea surface temperature (SST) variability in the ENSO region (e.g., Moron and Gouirand 2003; Bladé et al. 2008; King et al. 2018a; and others) as well as the intermediate role of the other tropical basins in the ENSO teleconnections using various observations and models (e.g., Ayarzagüena et al. 2018; Hardiman et al. 2019). During early winter, strong convection anomalies in the tropical western Pacific (TWP) tend to shape the ENSO-forced circulation anomalies over the Euro-Atlantic sector with relatively weaker forced Aleutian low in the North Pacific region, which becomes the canonical ENSO response in late winter because of the shifting of the tropical heating anomalies to the central-eastern equatorial Pacific region (e.g., Bladé et al. 2008). Moreover, the warming in the

Denotes content that is immediately available upon publication as open access.

Supplemental information related to this paper is available at the Journals Online website: https://doi.org/10.1175/JCLI-D-20-0075.s1.

Corresponding author: M. Adnan Abid, mabid@ictp.it

DOI: 10.1175/JCLI-D-20-0075.1

central-eastern equatorial Pacific (i.e., Niño-3.4 region) strongly influences the other ocean basins through atmospheric teleconnections; in particular it leads to anomalous heating and cooling in the Indian and Atlantic basins (e.g., Shinoda et al. 2004; Zhong et al. 2005; Cai et al. 2019; Abid et al. 2020), which provide additional sources of planetary-wave anomalies propagating into extratropical regions during boreal winter season (e.g., Ayarzagüena et al. 2018; Hardiman et al. 2019). This highlights the combined role of the ENSO and its interbasin teleconnection in modulating the intraseasonal variability of the extratropical circulation anomalies, particularly over the Euro-Atlantic region during boreal winter (e.g., Molteni et al. 2015; Scaife et al. 2017).

For the seasonal forecast to be skillful, it is important for the models to predict the teleconnections correctly between tropical and extratropical regions (e.g., Kumar et al. 2013), which are established through the Rossby wave excited from their tropical sources, also known as Rossby wave sources (RWS) (e.g., Hoskins and Karoly 1981; Sardeshmukh and Hoskins 1988). Recently, Scaife et al. (2017) revisited the North Atlantic Oscillation (NAO) seasonal forecast, where they show that tropical heating establishes its teleconnections to the Euro-Atlantic circulation anomalies through the Rossby wave propagation, with localized wave sources that lie between the edges of subtropical and the extratropical jet streams. During boreal winter, a significant RWS lies over the South Asia to East Asia region where a strong subtropical westerly jet exists, and any variation in predicting these wave sources may affect tropical–extratropical teleconnections, which establish through this "bridge" (Shimizu and de Albuquerque Cavalcanti 2011), and may consequently affect the model prediction skill. Therefore, the correct representation of the RWS in the models on intraseasonal time scale may improve the prediction skill of the Euro-Atlantic circulation anomalies, which is discussed in the current study.

Some other studies have shown that forcings from the tropical Indian and the Pacific Ocean counteract each other in generating circulation responses of opposite sign in the Euro-Atlantic region during the winter season (e.g., Fletcher and Cassou 2015; Fletcher and Kushner 2011). The warming in the western Indian Ocean enforces the positive NAO phase through the modification of the subtropical South Asian jet (SAJET), while cooling induces the negative NAO phase, during the boreal winter season on decadal and longer time scale (e.g., Bader and Latif 2005; Kucharski et al. 2006). However, the relevance of subtropical SAJET mechanism on interannual time scales (particularly during individual winter months) in connection with tropical heating from the Indian and the Pacific Ocean has yet to be established and is discussed in the current study.

King et al. (2018a) have shown a high intraseasonality of the ENSO response in the Euro-Atlantic region, with stronger linkage in early compared to the late winter. They proposed a few potential mechanisms to understand the intraseasonal characteristics of the ENSO teleconnections with the Euro-Atlantic region, one of which is ENSO–interbasin teleconnections. In this context, connections with the Atlantic Ocean have also been investigated to explain the extratropical ENSO response. Using seasonal hindcast and noninitialized coupled model simulations, Ayarzagüena et al. (2018) noted that an ENSO-forced secondary Rossby wave source located over the Gulf of Mexico and the Caribbean may excite Rossby wavetrains that modulate the Euro-Atlantic circulation anomalies. They showed that there is no transition between the early and late winter response to ENSO in free-running (noninitialized) models due to mean SST biases in comparison to observations, reanalyses, and initialized coupled models. These results highlighted the importance of the ENSO forced connections to the Atlantic basin and their role in seasonal predictions, even though the hindcast period (1993–2015) considered was relatively short. Another ENSO interbasin connection is with the Indian Ocean (e.g., Wang 2019). During boreal winter season, a warm ENSO phase enforces positive heating anomalies in the central-western Indian Ocean (e.g., Molteni et al. 2015). These Indian Ocean heating anomalies result in a positive NAO response over the Euro-Atlantic sector (Molteni et al. 2020). However, the role of the Indian Ocean forcing in the ENSO-response transition from early to the late winter in the Euro-Atlantic region has not yet been fully understood in the existing scientific literature.

Therefore, the goal of the present study is to investigate the relevance of the tropical heating from the central-eastern equatorial Pacific and the tropical Indian Ocean for the response of the Euro-Atlantic circulation anomalies during winter, and specifically their transition from early to late winter. The diagnostic analysis will be performed on both a reanalysis dataset from the European Centre for Medium-Range Weather Forecasts (ECMWF), namely ERA-Interim (Dee et al. 2011), and their Seasonal Forecast System 5 (SEAS5; Johnson et al. 2019) dataset for the period 1981–2015, which includes a limited number of ENSO events. Moreover, numerical experiments with an idealized tropical forcing pattern are performed with an intermediate complexity atmospheric global climate model (ICTP-AGCM; Molteni 2003; Kucharski et al. 2006, 2013).

The datasets and model used are described in section 2. The results of our investigations are presented and discussed in section 3, with a focus on the relative contribution of forcings from the Indian Ocean and the "traditional" ENSO region in the central-eastern tropical Pacific. A summary and conclusions are presented in section 4.

2. Datasets and model

a. *Reanalysis and observational dataset*

The ECMWF interim reanalysis (ERA-Interim; Dee et al. 2011) is used to assess the ENSO teleconnections over the Euro-Atlantic region. The reanalysis dataset for geopotential height and winds is available on a reduced Gaussian grid with approximately uniform latitude–longitude grid spacing of $0.75° \times 0.75°$ (~79 km) (Berrisford et al. 2011). A monthly global observed sea surface temperature (SST) dataset from the Hadley Centre (HadISST) was adapted; this is a combination of monthly observed global SSTs and sea ice concentration available from 1871 to the present on $1° \times 1°$ horizontal spatial resolution. In the current study, HadISST, which is a blend of the marine observations and in situ and satellite

information is used as observed SSTs for the period 1981–2015 (Rayner et al. 2003). For monthly observed precipitation, the Global Precipitation Climatology Project (GPCP) dataset is used for the period 1981–2015. The GPCP dataset is a merged analysis of the surface rain gauge stations, satellites, and sounding observations, available at 2.5° latitude × 2.5° longitude spatial horizontal resolution (Adler et al. 2003). As with every dataset, GPCP has some limitations, in this case because of the latitudinal satellite differences, which may add spatial heterogeneity to the dataset. However, GPCP is widely used as an observed precipitation in assessing global teleconnections (e.g., Scaife et al. 2017; Molteni et al. 2020). All the observational and reanalysis datasets are regridded to 1° latitude × 1° longitude spatial horizontal resolution.

Note that reanalysis is a combination of observations and the climate produced by numerical models, and it is used as an approximation of observations for the analysis of the present-day climate.

b. ECMWF-SEAS5 seasonal hindcast dataset

The seasonal hindcast data were obtained from the ECMWF SEAS5 (Johnson et al. 2019), which is based on the Integrated Forecast System (IFS) atmospheric model coupled to the Nucleus for Oceanic Modeling of the Ocean (NEMO) v4.5 ocean model. The atmospheric model resolution is T319 with a cubic octahedral grid, 91 vertical levels, and a model top at 0.01 hPa, while the horizontal resolution of the ocean model is ORCA0.25 with 75 vertical ocean levels. The coupled system also includes the Louvian-la-Neuve Sea Ice Model (LIM2) with ORCA 0.25° resolution and a wave model at 0.5°. For each year, the atmospheric initial conditions are from ERA-Interim, while the ocean was initialized using Ocean Reanalysis System 5 (ORAS5). The land, soil, and snow initializations were made based on the forced 43r1 land surface model. A total of 25 ensemble members are available for the period 1981–2015, each member starting from the first day of each calendar month and integrated for the next 7 months. In the current study, we used reforecasts initialized on 1 November, available at 1° × 1° resolution from the Copernicus Climate Change Service portal (https://climate.copernicus.eu). The seasonal hindcast dataset is used to analyze the model's ability in predicting the Euro-Atlantic circulation anomalies response transition to ENSO from early to late winter, which consequently will impact its seasonal prediction skill.

c. Wave activity analysis

The Rossby wave source, along with its propagation and direction emanating from the tropical sources, is diagnosed using Takaya and Nakamura's (2001) wave activity flux method. It is considered a useful tool that provides an information about the wave propagation independent of its phase but parallel to local group velocity of the stationary Rossby wave packet (Takaya and Nakamura 2001; Honda et al. 2009; McIntosh and Hendon 2018).

$$W = \frac{p\cos\phi}{2|U|}\left\{\begin{array}{l} \dfrac{u}{a^2\cos^2\phi}\left[\left(\dfrac{\partial\psi'}{\partial\lambda}\right)^2 - \psi'\dfrac{\partial^2\psi'}{\partial\lambda^2}\right] + \dfrac{v}{a^2\cos\phi}\left(\dfrac{\partial\psi'}{\partial\lambda}\dfrac{\partial\psi'}{\partial\phi} - \psi'\dfrac{\partial^2\psi'}{\partial\lambda\,\partial\phi}\right) \\ \dfrac{u}{a^2\cos\phi}\left(\dfrac{\partial\psi'}{\partial\lambda}\dfrac{\partial\psi'}{\partial\phi} - \psi'\dfrac{\partial^2\psi'}{\partial\lambda\,\partial\phi}\right) + \dfrac{v}{a^2}\left[\left(\dfrac{\partial\psi'}{\partial\phi}\right)^2 - \psi'\dfrac{\partial^2\psi'}{\partial\phi^2}\right] \\ \dfrac{f_0^2}{N^2}\left[\dfrac{u}{a\cos\phi}\left(\dfrac{\partial\psi'}{\partial\lambda}\dfrac{\partial\psi'}{\partial z} - \psi'\dfrac{\partial^2\psi'}{\partial\lambda\,\partial z}\right) + \dfrac{v}{a}\left(\dfrac{\partial\psi'}{\partial\phi}\dfrac{\partial\psi'}{\partial z} - \psi'\dfrac{\partial^2\psi'}{\partial\phi\,\partial z}\right)\right] \end{array}\right\} \tag{1}$$

In Eq. (1), p is the pressure, f_0 is the Coriolis parameter at 45°N, a is Earth's radius, N is the Brunt–Väisälä frequency, ϕ is the latitude, and λ is the longitude. The perturbed geostrophic streamfunction ψ' is defined as φ/f, where φ is the geopotential height and $f = 2\Omega\sin\phi$ is the Coriolis parameter with Ω the Earth's rotation rate. Finally, $|U|$ is the wind speed of the basic flow, while u and v are the climatological zonal and meridional winds, respectively.

d. Numerical model simulations

Additionally, the intermediate complexity International Centre for Theoretical Physics Atmospheric Global Climate Model (ICTP-AGCM), named SPEEDY, is used to investigate the sensitivity of the Euro-Atlantic circulation anomalies response to the heating anomalies in the Indian Ocean. The ICTP-AGCM is widely used for the climate variability and predictability studies over the extratropical region (e.g., Kucharski et al. 2006; Herceg-Bulić et al. 2012; Abid et al. 2015; Ruggieri et al. 2017, and many others) as well as over the monsoonal regions (e.g., Feudale and Kucharski 2013, and others). SPEEDY uses T30 (~3.75° × 3.75°) spatial resolution with eight vertical levels, which makes the model computationally quite inexpensive, with reasonably well-simulated global climatological features compared to those of observations. For further details please see the following link: http://users.ictp.it/~kucharsk/speedy-net.html. In SPEEDY, convective processes are determined through a mass-flux scheme, the boundary layer fluxes are parameterized by stability-dependent bulk formulas, while radiation is represented through shortwave and longwave radiation parameterizations. Moreover, a simplified one-layer thermodynamic model is used to determine land and sea ice temperature anomalies (Kucharski et al. 2013).

e. Methodology

The regression maps are calculated as covariance of a normalized anomaly index with a global anomaly field (e.g., Molteni et al. 2015). The partial regression method was used to analyze the influence of the different tropical forcings on the

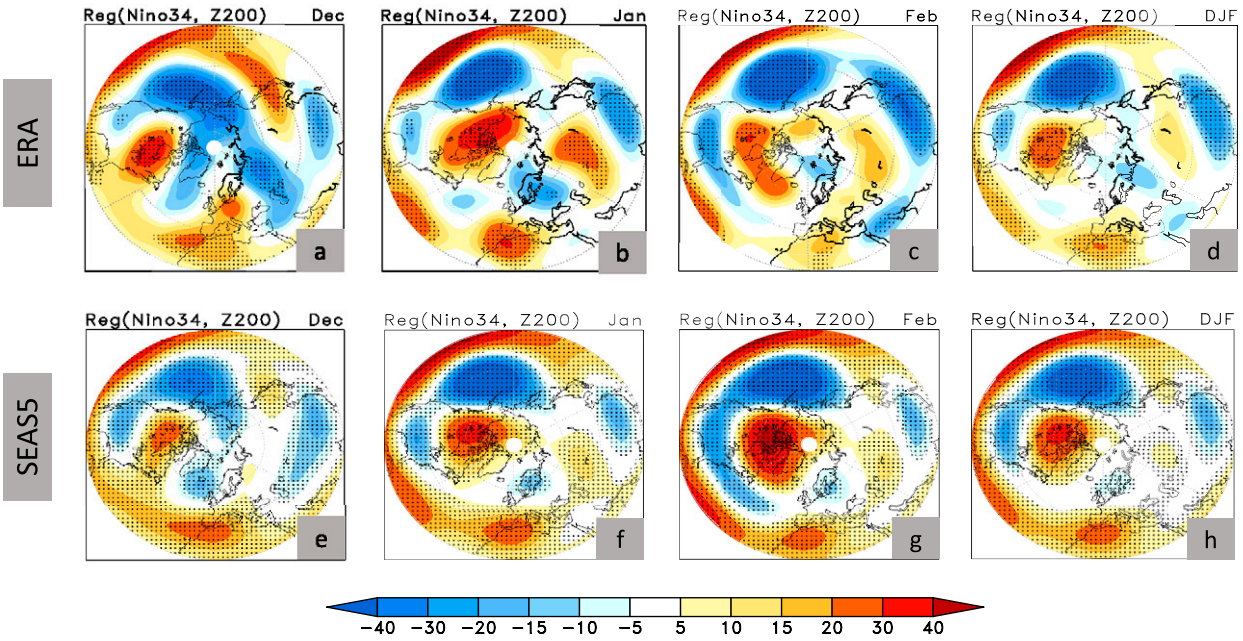

FIG. 1. (a)–(c) Regression of monthly reanalysis (ERA-Interim) 200-hPa geopotential height anomalies (m) onto the observed corresponding Niño-3.4 SST index for the period 1981–2015. (e)–(g) As in (a)–(c), but for the ECMWF-SEAS5. (d) Reanalysis DJF mean 200-hPa geopotential height anomalies (m) regressed onto the observed Niño-3.4 DJF SST index for the period 1981–2015. (h) As in (d), but for SEAS5. Spatial correlation is 0.77, 0,85, 0.82, and 0.91, respectively. Stippling denotes statistical significance at the 95% confidence level.

Euro-Atlantic circulation anomalies (e.g., Kucharski et al. 2009; Cai et al. 2011) Furthermore, a two-tailed Student's *t* test is applied to test the statistical significance of the results. The statistical significance for the SEAS5 ensemble prediction dataset was estimated from the standard deviation derived from the inter-ensemble spread of the regression coefficients.

3. Results and discussion

a. The response to ENSO in early and late winter

The reanalysis (ERA-Interim) and SEAS5 model responses of the 200-hPa geopotential height to their corresponding area-averaged SST anomalies from the central-eastern equatorial Pacific (190°–240°E, 5°S–5°N) region (Niño-3.4 index) during the boreal winter (December–February) season for the period 1981–2015 are shown in Fig. 1. The monthly reanalysis (ERA) 200-hPa geopotential height anomalies are regressed onto the corresponding Niño-3.4 SST index from December to February for the period 1981–2015 (Figs. 1a–c) and compared with the 3-monthly seasonal mean reanalysis response for the same period (Fig. 1d). Similarly, the SEAS5 predicted monthly 200-hPa geopotential height anomalies from December to February are regressed onto the corresponding Niño-3.4 SST index for each ensemble member separately, and then the mean over all the ensemble members is computed. These monthly regressions are shown in Figs. 1e–g respectively for three winter months and compared with the regression computed from the predicted seasonal mean (3-month mean) of the 200-hPa geopotential height anomalies onto the corresponding Niño-3.4 SST index (Fig. 1h). An upper-level geopotential height gradient with positive anomalies over the subtropical Atlantic and negative anomalies over the northern Atlantic region appears during December for both reanalysis and SEAS5 (Figs. 1a and 1e respectively), which resembles the positive NAO-like pattern. A shift in the anomalous pattern happens in January (Figs. 1b,f), where positive NAO weakens, whereas over the North Pacific sector the Aleutian low and the North American high strengthen in late winter (February; Figs. 1c,g), which is stronger in SEAS5 with a similar strength of the Aleutian low (Fig. 1g) compared to the reanalysis (Fig. 1c). The late winter (February) pattern shows a stronger Pacific–North American (PNA)-like anomaly over the North American sector compared to the early winter (December), which projects weakly (statistically insignificant) onto the negative NAO phase (Fig. 1c) over the North Atlantic sector. Averaging over 3 months (DJF) weakens the ENSO forced wave train over the Euro-Atlantic sector (Fig. 1d), which is also reproduced by the SEAS5 prediction dataset (Fig. 1h). The weakening of the seasonal mean (DJF) response point toward the strong intraseasonality of the ENSO teleconnections with the Euro-Atlantic sector as also seen in each month teleconnection pattern.

The spatial pattern correlation between the reanalysis and SEAS5 regressed 200-hPa circulation anomalies averaged over the Northern Hemisphere (NH) region (20°–85°N, 0°–360°E) is higher during the late winter (February: 0.91) compared to the earlier winter (December: 0.71) due to the stronger direct

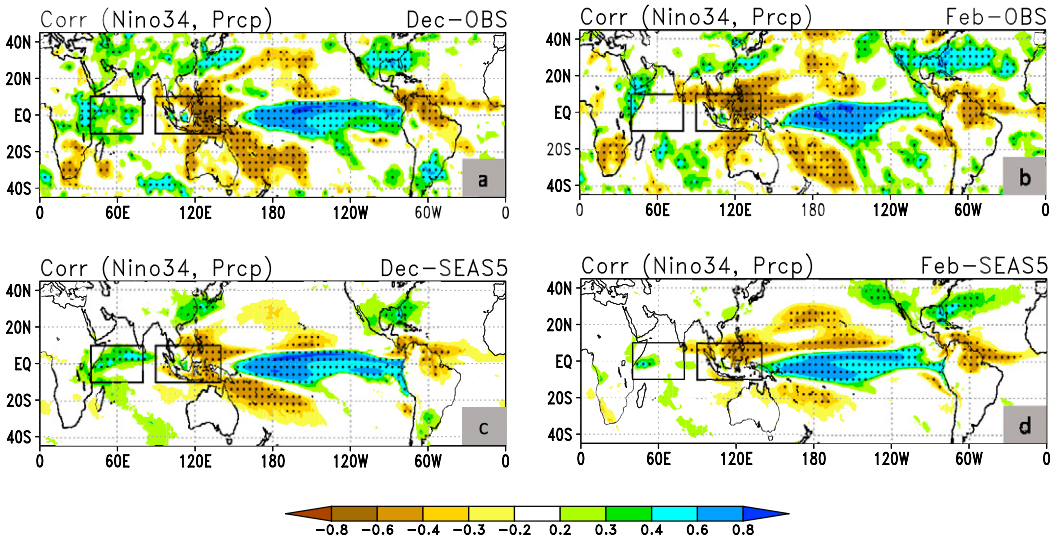

FIG. 2. (a),(b) Correlation of the observed Niño-3.4 SST index with their corresponding observed precipitation for December and February respectively for the period 1981–2015, (c),(d) As in (a) and (b), but for ECMWF-SEAS5. Two boxes highlight the western (40°–80°E, 10°S–10°N) and eastern Indian Ocean (90°–140°E, 10°S–10°N) domains used for the tropical western–eastern Indian Ocean (TWEIO) precipitation index. Stippling denotes statistical significance at the 95% confidence level.

ENSO influences over the extratropical region in late winter. Moreover, the SEAS5 predicts reasonably well the NH teleconnection in comparison to the previous cycle SEAS4 (King et al. 2018a, their Fig. 4), with about 25% higher monthly spatial correlation. King et al. (2018a) proposed various possible mechanisms for the transition of the ENSO early to late winter teleconnections in the Euro-Atlantic sector. In the current study, we address one of the proposed mechanisms, namely the changing ENSO interbasin atmospheric teleconnections from early to late winter and their role in the phase transition of the circulation anomalies over the Euro-Atlantic sector.

To analyze the ENSO interbasin teleconnections, the observed and the SEAS5 predicted Niño-3.4 SST indices are correlated in early (December) and late winter (February) with their corresponding global precipitation respectively (Fig. 2). Figure 2a shows the relationship between the observed precipitation anomalies and the corresponding Niño-3.4 SST index in December, which extends from the Pacific to the Indian and the Atlantic basins. A tripolar precipitation pattern appears in the equatorial Pacific and Indian Ocean with two positive anomalous centers located in the central-eastern equatorial Pacific and in the tropical western Indian Ocean (TWIO) regions, while a third center with negative anomalies is located over the tropical eastern Indian Ocean (TEIO) extending to the tropical western Pacific (TWP) region; this is consistent with the seasonal-mean teleconnections computed by Molteni et al. (2015). This ENSO–Indian Ocean relationship becomes weaker in late winter (February), while significant anomalies appear in the subtropical Atlantic region (Fig. 2b), compared to the early winter (Fig. 2a).

For the SEAS5, the correlation of the Niño-3.4 SST index with the global precipitation is calculated for each ensemble member separately, and then the average correlation of 25 ensemble members is calculated after applying the Fisher Z transformation; results are shown for early (December; Fig. 2c) and late winter (February; Fig. 2d), respectively. The SEAS5 shows the tripolar tropical precipitation structure (Fig. 2c) similar to that of observation (Fig. 2a) in early winter, while some differences are noted in late winter teleconnection pattern particularly over the tropical Indian Ocean as well as in equatorial Pacific region, where warm anomalies are extended westward (Fig. 2d) compared to the observations (Fig. 2b). During early winter (December), the prediction skill of the area-averaged precipitation anomalies over the TWIO (40°–80°E, 10°S–10°N) is 0.65 and for the TEIO (90°–140°E, 10°S–10°N) is 0.80, which is low compared to that of Niño-3.4 precipitation index (0.95). Overall, the SEAS5 predicts the transition of the ENSO interbasin atmospheric teleconnection from early to late winter quite well in the tropical Indian Ocean as well as in the Atlantic Ocean, although with some biases in the latter area in its ENSO teleconnections.

The tropical forcing is mainly determined by precipitation anomalies, through latent heat release that determines the Rossby wave source; they are useful for the assessment of the teleconnections (e.g., Molteni et al. 2015). To further investigate the tripolar precipitation structure and its atmospheric teleconnections, a tropical Indian precipitation dipole index area-averaged over the tropical western (40°–80°E, 10°S–10°N)–tropical eastern Indian Ocean (90°–140°E, 10°S–10°N) region (namely TWEIO; boxes indicated in Fig. 2a) is defined, while a Niño-3.4 precipitation index is defined for the precipitation anomalies area-averaged over the central-eastern equatorial Pacific region. The comparative role of the two oceanic indices (TWEIO and Niño-3.4) in modulating the

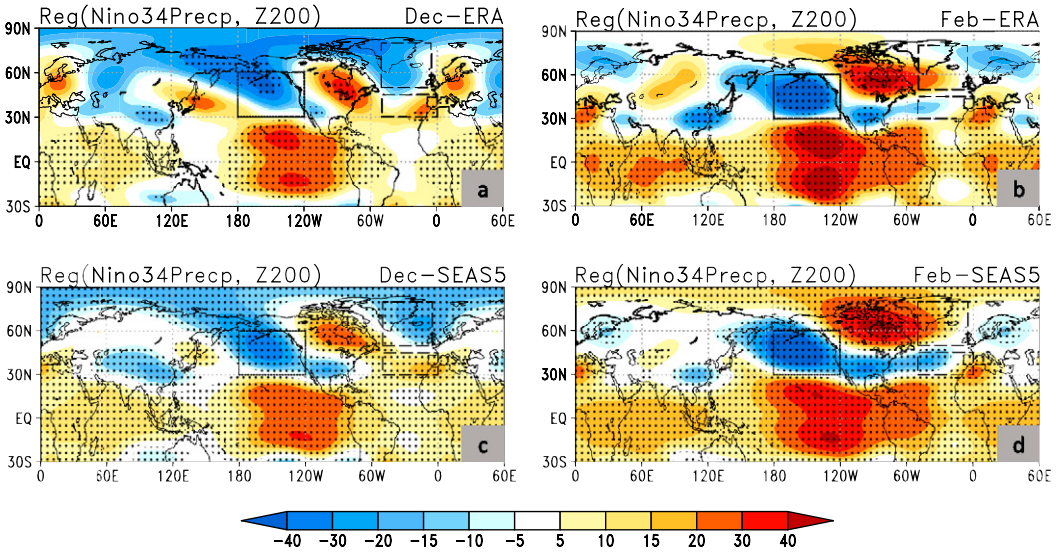

FIG. 3. (a),(b) Regression of reanalysis 200-hPa geopotential height anomalies (m) onto their corresponding observed Niño-3.4 precipitation anomalies index for December and February, respectively, for the period 1981–2015. (c),(d) As in (a) and (b), but for ECMWF-SEAS5. Stippling denotes statistical significance at the 95% confidence level. Boxes in North Atlantic sector are used to define the NAO index, while the box over the North Pacific sector is used to define the Aleutian low index.

Euro-Atlantic circulation anomalies transition from early to late winter is discussed in detail in the following. It is pertinent to mention here that the TWEIO precipitation index used in this study is different from that defined in Annamalai et al. (2007), where the authors considered January to March as winter season, and from the classical Indian Ocean dipole (Saji et al. 1999).

Figure 3 shows the regression of the reanalysis 200-hPa geopotential height for early (December) and late winter (February) onto their respective observed normalized precipitation index from the Niño-3.4 region for the period 1981–2015. During early winter (Fig. 3a), negative geopotential height anomalies appear over the Arctic and North Atlantic region, and positive geopotential height anomalies over the subtropical Atlantic extended to the central-eastern European sector, which resembles a positive NAO-like pattern. A canonical ENSO response appears (Fig. 3b) in late winter (February), closer to a positive PNA-like pattern compared to the early winter (December). In February, a weaker negative NAO like pattern (statistically insignificant) appears over the North Atlantic sector, with positive anomalies over the North Atlantic (north of about 50°N) and negative to its south at around 35°N (Fig. 3b). These results are similar to those obtained using the Niño-3.4 index defined using SSTs (Fig. 1). For the SEAS5 predictions, the Niño-3.4 regression pattern is calculated for each ensemble member separately and then the ensemble-mean regression pattern is computed for December (Fig. 3c) and February (Fig. 3d), respectively. The SEAS5 predictions show the transition of the Euro-Atlantic circulation anomalies from early (Fig. 3c) to late winter (Fig. 3d) quite well compared to the reanalysis. To quantify the Euro-Atlantic circulation anomalies responses to the ENSO as well as to Indian Ocean forcing, we define a 200-hPa geopotential height anomalies-based NAO index over the Euro-Atlantic sector. The difference of the 200-hPa geopotential height anomalies area-averaged over Iceland (310°–355°E, 50°–80°N) and the Azores (310°–360°E, 30°–45°N)—shown with the two boxes over the North Atlantic sector; Fig. 3—mimics the NAO index over the North Atlantic sector.

The ENSO-forced NAO index is 28.3 m for reanalysis and 24.1 m for SEAS5 in December, whereas it is −9.0 m for reanalysis and −14.8 m for SEAS5 in February. Considering 1-sigma (12.7-m standard deviation) spread around the ensemble mean for SEAS5, the reanalysis NAO lies within the ensemble spread during December (Fig. S1 in the online supplemental material). Moreover, the large spread among the SEAS5 ensemble members could be contributed from internal atmospheric variability (Deser et al. 2018). During late winter (Figs. 3b,d), the strengthening of the Aleutian low in reanalysis as well as in SEAS5 is because of the direct poleward ENSO response (e.g., Hoskins and Karoly 1981; Bladé et al. 2008). The area-averaged 200-hPa geopotential height anomalies over the Aleutian low (180°–240°E, 30°–60°N) region (shown as the box over the North Pacific region in Fig. 3) defines the Aleutian low index, which strengthens about 50% from early to late winter in reanalysis, while ~40% strengthening of the Aleutian low is noted in SEAS5. During late winter, the deepening of the Aleutian low increases the wave activity flux from the North Pacific into the North Atlantic sector as well as into the stratosphere, which may trigger the negative NAO pattern over the Euro-Atlantic sector through a northern annular mode (NAM) response (e.g., Thompson and Wallace 2000; Hitchcock and Simpson 2014; Butler et al. 2014; Ineson and Scaife 2009; Toniazzo and Scaife 2006).

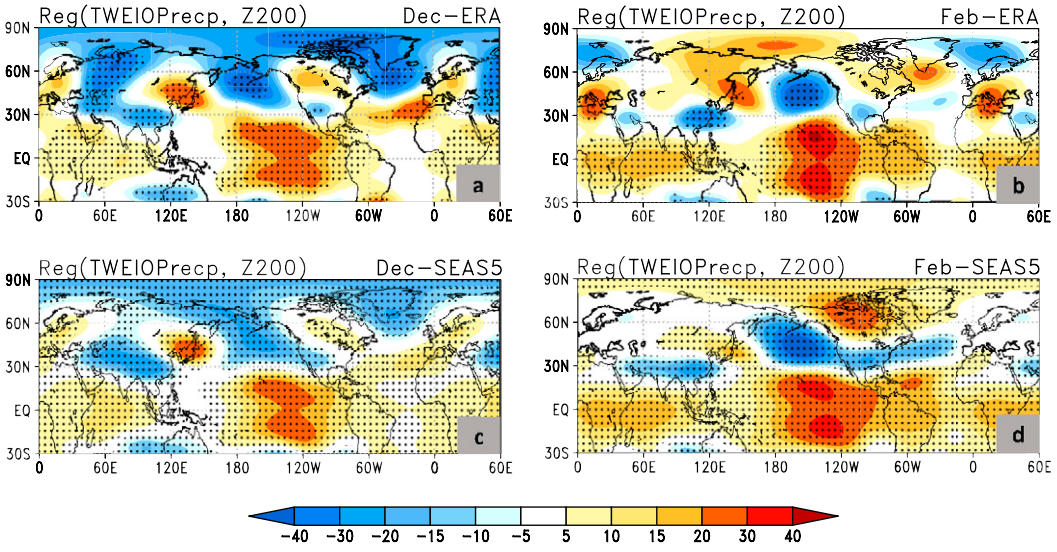

FIG. 4. (a),(b) As in Figs. 3a and 3b, but with observed TWEIO precipitation anomalies index. (c),(d) As in Figs. 3c and 3d, but with the TWEIO ECMWF-SEAS5 index. Stippling denotes statistical significance at the 95% confidence level.

The tropical Indian Ocean heating anomalies are positively correlated with the NAO during the boreal winter season (Yu and Lin 2016; Scaife et al. 2017; Lee et al. 2019). To investigate the robustness of this relationship, the reanalysis 200-hPa geopotential height anomalies are regressed onto the observed normalized TWEIO precipitation index during December (Fig. 4a) and February (Fig. 4b) respectively. Similarly, the SEAS5 200-hPa geopotential height anomalies are regressed onto the corresponding TWEIO index and the ensemble mean response for December and February as shown in Figs. 4c and 4d respectively. The TWEIO regression patterns show similarities to those of the Niño-3.4 regression patterns (Fig. 3), particularly in early winter (December). The TWEIO-forced reanalysis NAO index is 43.8 m (Fig. 4a), which is about 55% stronger than the Niño-3.4 forced pattern (Fig. 3a) in early winter (December), while not much difference appears in the NAO pattern forced from the Indian Ocean (−9.2 m; Fig. 4b) and from the Niño-3.4 (−9.0 m; Fig. 3b) in late winter (February). However, the SEAS5-based positive NAO response to the TWEIO (22.0 m; Fig. 4c) is almost similar to the ENSO (24.1 m; Fig. 3c) forcings in early winter, but a significant difference appears for late winter negative NAO response to the ENSO forcing (−14.8 m; Fig. 3d) compared to the Indian Ocean forcing (−8.5 m; Fig. 4d). In particularly, in contrast to reanalysis in SEAS5 there is a weaker response in early winter from the Indian Ocean compared to the ENSO response.

Moreover, in early winter (December), a weaker positive correlation is noted between reanalysis NAO and Niño-3.4 index (0.24), while a relatively stronger and statistically significant (95% confidence level) correlation is found between TWEIO and NAO (0.38). However, for SEAS5 the correlation between NAO and TWEIO is 0.22, whereas with the Niño-3.4 index it is 0.24, which shows a similarity in NAO response to the Indian Ocean as well as the ENSO forcing in the prediction dataset. The ensemble mean–based SEAS5 NAO index correlations with the Niño-3.4 and the TWEIO are similar (0.63; statistically significant at 95% confidence level). The higher correlation in the ensemble mean is a result of its reduced internal variability. The statistically significant positive correlation in reanalysis indicates a stronger positive NAO-forced response to the Indian Ocean (Fig. 4a) compared to that of ENSO (Fig. 3a) in early winter. In early winter (December), the positive relationships of NAO with both tropical basins are consistent with earlier findings (e.g., Scaife et al. 2017). In the next section, the impact of the two tropical forcings from Niño-3.4 and the TWEIO to the Euro-Atlantic circulation anomalies will be analyzed independently.

b. *Role of forcing from different tropical regions: Pacific versus Indian Ocean*

In this section, the role of the tropical forcings from the Indian and Pacific Oceans in modulating the Euro-Atlantic atmospheric circulation anomalies is explicitly discussed by isolating their effect independently from each other; this is achieved using a partial regression method (e.g., Kucharski et al. 2009) as shown in Eq. (2):

$$X(t)_{\text{res}} = X(t) - b \times X(t)_{\text{RM}}. \tag{2}$$

Here, b is the least squares regression coefficient between the anomaly index time series $X(t)_{\text{RM}}$ (Niño-3.4 or TWEIO indices) to be removed and the anomaly index time series $X(t)$ (TWEIO or Niño-3.4 indices), while $X(t)_{\text{res}}$ is the residual time series, which is uncorrelated with $X(t)_{\text{RM}}$. In this way we can create a Niño-3.4 precipitation index linearly independent of the TWEIO index and a TWEIO precipitation index independent of the Niño-3.4 index. These indices will be called "pure Niño-3.4" and "pure TWEIO" for convenience in the following.

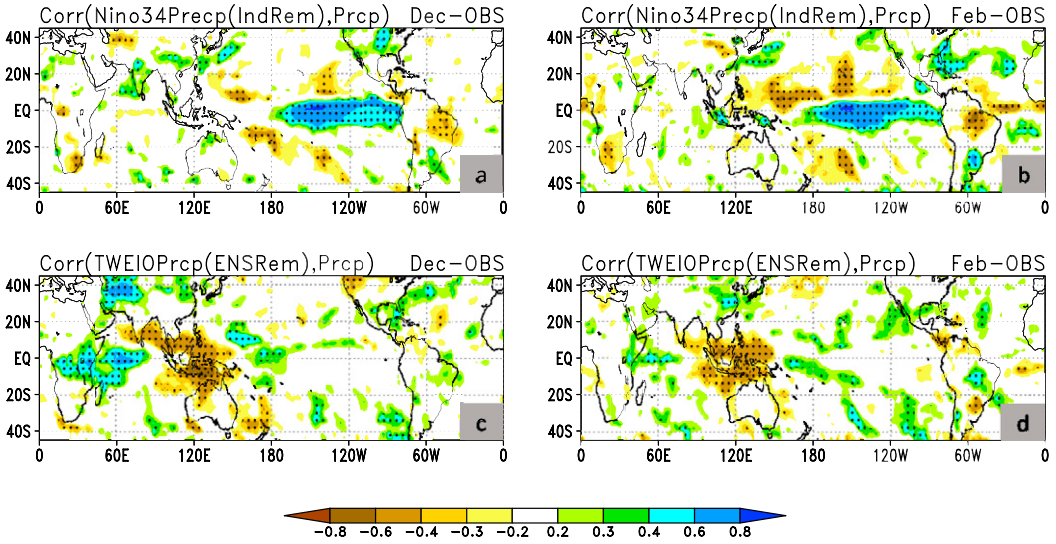

FIG. 5. (a),(b) Correlation of the observed pure Niño-3.4 precipitation anomalies index (after removing TWEIO) with the corresponding global precipitation anomalies for December and February respectively for the period 1981–2015. (c),(d) As in (a) and (b), but with pure TWEIO precipitation anomalies index (after removing Niño-3.4) for the period 1981–2015. Stippling denotes statistical significance at the 95% confidence level.

The observed pure Niño-3.4 precipitation index (independent of the TWEIO index) and pure TWEIO precipitation index (independent of the Niño-3.4 index) are correlated with the global precipitation shown in Figs. 5a and 5c respectively for early winter (December). These maps show that Niño-3.4 precipitation anomalies may occur without strong precipitation anomalies in the tropical Indian Ocean (Fig. 5a), as well as the tropical Indian Ocean precipitation dipole anomalies without strong anomalies in the central-eastern equatorial Pacific region (Fig. 5c) in early winter (December). The correlation between Niño-3.4 index and TWEIO is 0.64, which explains about 40% of the total variance of TWEIO, while it shows that about 60% of the TWEIO variability can exist independently of ENSO in early winter (December). In February, almost no signal is noted in tropical Indian Ocean with pure Niño-3.4 forcing (Fig. 5b), while with the pure TWEIO a much weaker signal appears, particularly over the western Indian Ocean (Fig. 5d) compared with the December map (Fig. 5c). The reason for the weakening of the signal in the Indian Ocean is likely related to a substantial southward shift of the climatological precipitation from December to February (Fig. S2), leading to much less precipitation near the equator in February compared to December.

Figure 6a shows the regression of the reanalysis 200-hPa geopotential height anomalies onto the pure observed Niño-3.4 precipitation index, which reveals almost 100% weaker and less significant ENSO teleconnection with the NAO (0.31 m) in the Euro-Atlantic region during December, compared to the total forcing (Fig. 3a). Also, compared to Fig. 3a, about 45% weaker Aleutian low response (−10.1 m) is found over North Pacific, while wider positive height anomalies appear over eastern North America, and the eastern European region (Fig. 6a). However, during late winter (February), the 200-hPa geopotential height anomalies connected with the pure Niño-3.4 (Fig. 6b; NAO −11.9 m) resemble to those of total pattern (Fig. 3b; −14.8 m). This suggests that the atmospheric teleconnections in February are mainly forced by the ENSO signal, rather than by its interbasin teleconnections.

Next, the reanalysis 200-hPa geopotential height anomalies for December are regressed onto the observed pure TWEIO precipitation index (Fig. 6c). A strong upper-level negative geopotential height anomaly over the Euro-Atlantic region and positive over the subtropical Atlantic region appear in Fig. 6c; this dipole resembles a positive NAO pattern (33.5 m), which is much stronger than purely ENSO forced (0.31 m) pattern (Fig. 6a), consistent to that found using the total forcings (Figs. 3a and 4a). This analysis reveals that a substantial part of the ENSO induced Euro-Atlantic circulation anomalies is not directly forced by heating anomalies from the central-eastern equatorial Pacific (Niño-3.4) region, but the tropical Indian Ocean provides the primary forcing to the positive NAO like pattern during early winter. On the other hand, in late winter (February; Fig. 6d) the pure TWEIO-forced 200-hPa geopotential height anomalies show significant differences over the North American and North Pacific region with weakening (~80%) of Aleutian low, projecting weakly onto the negative NAO (about 45% weaker) with respect to the full TWEIO regression (Fig. 4b). This indicates that the PNA pattern is mainly modulated by the ENSO anomalies from the central-eastern equatorial Pacific region.

The SEAS5 also shows a response broadly similar to the reanalysis for the two independent tropical precipitation forcings (Fig. 7). With pure Niño-3.4 (Fig. 7a) the positive NAO (13.4 m) is about 40% weaker in early (December), while negative NAO (−11.9 m) is about 20% weaker in late winter (Fig. 7b; February) compared to the full Niño-3.4 regressions

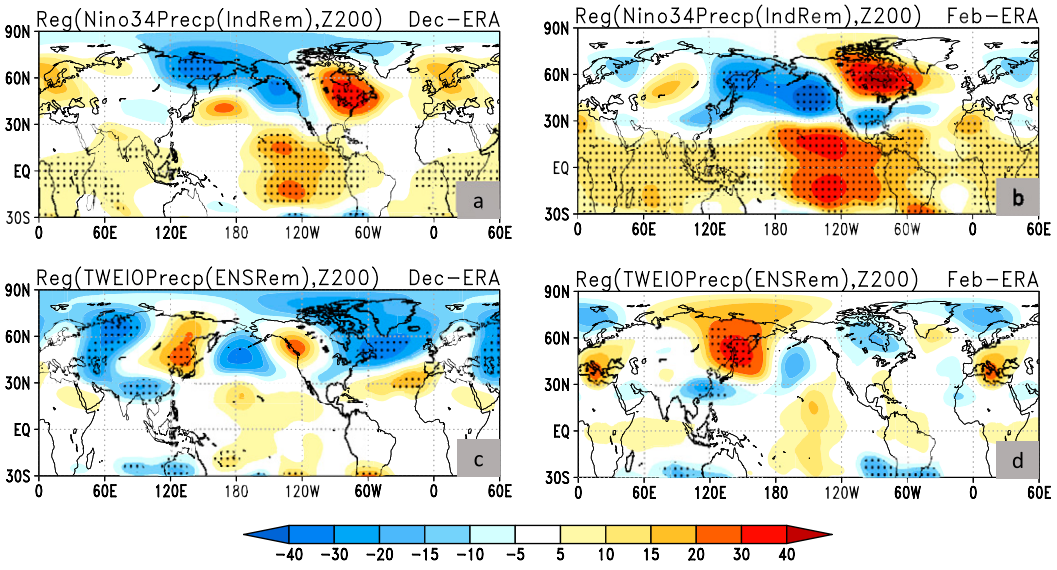

FIG. 6. (a),(b) Regression of December and February reanalysis 200-hPa geopotential height anomalies (m) onto the corresponding observed pure Niño-3.4 precipitation anomalies index (after removing TWEIO) for the period 1981–2015. (c),(d) As in (a) and (b), but with observed pure TWEIO precipitation anomalies index (after removing the Niño-3.4 region). Stippling denotes statistical significance at the 95% confidence level.

(Figs. 3c,d). The NAO (10.5 m) forced with the pure Indian Ocean is nearly 50% weaker in magnitude in early (Fig. 7c) and it almost vanishes NAO (−0.53 m) in late winter (Fig. 7d) compared to the full TWEIO regressions (Figs. 4c,d). SEAS5 shows a similar response in the positive NAO to the two pure forcing (Figs. 7a,c) with a slightly (~20%) dominating role of ENSO compared to the Indian Ocean in early winter. Moreover, in early winter, the positive NAO response to the pure Indian Ocean forcing is clear and stronger in the reanalysis (Fig. 6c) compared to SEAS5 (Fig. 7c). Overall, the SEAS5 predictions captures the early to late winter NAO transition to some extent, with relatively weaker Indian Ocean teleconnections compared to the reanalysis. The results shown in Figs. 6 and 7 are an important basis for the rest of our investigation.

To better identify the planetary wave propagation in the early winter (December), the wave activity flux (WAF) is regressed onto the pure TWEIO index for reanalysis (Fig. 8a)

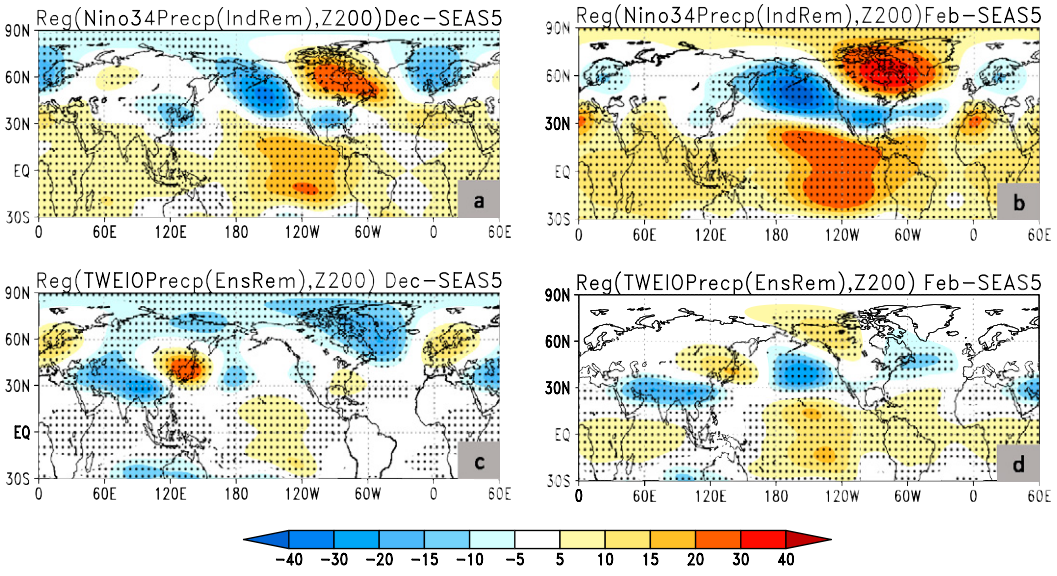

FIG. 7. As in Fig. 6, but for the ECMWF-SEAS5. Stippling denotes statistical significance at the 95% confidence level.

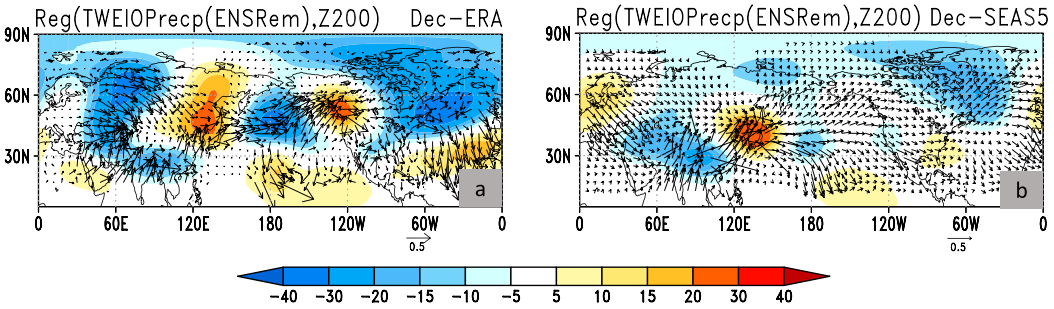

FIG. 8. (a) Regression of reanalysis of December 200-hPa geopotential height anomalies onto the observed pure TWEIO precipitation index (shaded; m), and the vector ($m^2 s^{-2}$) corresponds to the wave activity flux (WAF) for the period 1981–2015. (b) As in (a), but with ECMWF-SEAS5.

as well as for SEAS5 (Fig. 8b) respectively. The WAF defines the wave path emanating from its tropical source, which is parallel to its group velocity and is also consistent with its ray path (e.g., McIntosh and Hendon 2018). The vectors indicate the source of the originating wave from the Indian Ocean around 20°N, it reaches eastern China where a divergent center appears, and then move eastward to the North Pacific sector (around the date line at 40°N), then crossing North America and reaches to the North Atlantic sector south of the Greenland region. It corresponds to a wavenumber-3-like pattern emanating from the subtropical South Asia region, which propagates through the North Pacific and North America and impacts the Euro-Atlantic region (Fig. 8a). Over the North Pacific sector some part of the wave shows divergent behavior propagating toward the equatorial region. The SEAS5 reproduces a response similar to the reanalysis but with notably weaker amplitude over both the North Pacific and the North Atlantic sector (Fig. 8b). Although the SEAS5 predicts the phase of the tropical–extratropical teleconnection reasonably well in comparison to the reanalysis, the wave is weaker in amplitude, which has implications for the predictability of the Euro-Atlantic circulation anomalies as noted in Fig. 7c. The results in Figs. 6–8 suggest that the Indian Ocean teleconnection with ENSO is responsible for the apparent transition of the ENSO-forced circulation anomalies in the Euro-Atlantic region from early to late winter, with Indian Ocean precipitation being the primary source of the positive NAO signal observed in early winter.

The Indian Ocean competes with ENSO forcing in its influences on the stratospheric circulation anomalies through meridional eddy heat fluxes during boreal winter (e.g., Fletcher and Kushner 2011). To investigate the stratospheric responses we used the pure TWEIO precipitation index and pure Niño-3.4 index according to Eq. (2) and regressed them with 10-hPa geopotential height anomalies to analyze the influence of the two tropical forcings separately on the northern annular mode (NAM) also known as Arctic Oscillation (AO) (Thompson and Wallace 2000). In early winter, a positive AO-like response to the Indian Ocean forcing is seen (see Fig. S3c), while the response to the pure Niño-3.4 (Fig. S3a) forcing in the polar cap region is a wavenumber 1. On the other hand, in February, negative AO-like circulation anomalies appear with wavenumber-2 response to the pure Niño-3.4 forcing (Fig. S3b), while the pure TWEIO forcing induces positive AO circulation anomalies (Fig. S3d). The AO index response is quantified as the area-averaged difference between the two centers [(35°–55°N, 0°–360°E) − (65°–90°N, 0°–360°E)], identified from the leading mode of an empirical orthogonal function (EOF) applied to the 10-hPa geopotential height north of 20°N. The positive AO response to the TWEIO is prominent in early (December; 118.3 m) compared to the late winter (February; 10.1 m), while Niño-3.4 forces a stronger negative AO circulation anomaly in late (−83.0 m) compared to early winter (−17.7 m). This is consistent with earlier findings (e.g., Ineson and Scaife 2009; Butler et al. 2014). Moreover, the AO index correlation with the Indian Ocean (TWEIO) is 0.37 (statistically significant at 95% confidence level), while the correlation with the Niño-3.4 index is 0.20. This confirms the dominant role of the Indian Ocean compared to the Niño-3.4 forcing in early winter. However, in late winter a weaker AO correlation is found with the Niño-3.4 forcing (−0.19), which dominates over the response to the Indian Ocean forcing. In summary, the stratospheric response in the polar cap region is dominated by the Indian Ocean in early winter, whereas the ENSO response dominates in late winter by inducing a negative AO response (e.g., Fletcher and Kushner 2011; Hitchcock and Simpson 2014; Hardiman et al. 2019).

c. *Connection with the subtropical South Asian jet*

Figure 8 shows a wave train emanating from subtropical South Asia enforces the positive NAO like pattern over the Euro-Atlantic region in early winter. Further analysis was carried out to understand the teleconnection between the Indian Ocean and the Euro-Atlantic region in early winter. The TWEIO precipitation dipole index was correlated with the 200-hPa zonal (U) winds in December; a significant positive correlation was found within 20°–40°N, 30°–80°E, which shows a strengthening of the subtropical South Asian jet (SAJET) during early winter due to the Indian Ocean heating dipole. (Fig. 9a).

Following Bader and Latif (2005), a 200-hPa subtropical South Asian jet index (SAJETI; 40°–80°E, 22°–37°N) was defined using reanalysis zonal U winds during December. The correlation between observed TWEIO precipitation dipole index and SAJETI is 0.60 (statistically significant at 95% confidence level), which shows a strong covariability among them in early winter. The 200-hPa geopotential height anomalies

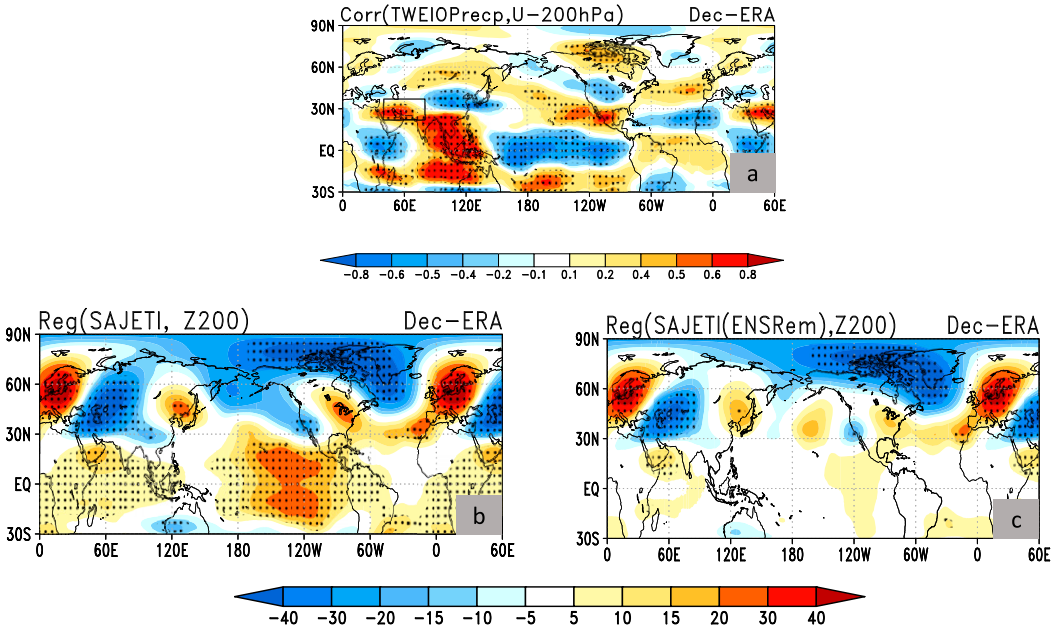

FIG. 9. (a) Correlation of the observed TWEIO precipitation index with the reanalysis 200-hPa zonal winds *U* for the period 1981–2015. The box highlights the South Asian jet index (SAJETI) over the region 40°–80°E, 22°–37°N. (b) Regression of 200-hPa geopotential height anomalies (m) onto SAJETI. (c) As in (b), but with SAJETI (after removing the Niño-3.4 influence). Stippling denotes statistical significance at the 95% confidence level.

are regressed onto this SAJET index for early winter (Fig. 9b). A wavenumber-3 pattern appears with a positive NAO-like anomaly over the Euro-Atlantic region similar to that of Figs. 4a and 6c, suggesting that SAJET acts as an atmospheric bridge between the forcing from the tropical Indian Ocean and extratropical wave pattern, which affects the Euro-Atlantic circulation anomalies during early winter. Moreover, the SEAS5 200-hPa geopotential height anomalies are regressed onto SAJETI for each member of the ECMWF SEAS5 ensembles. The ensemble-mean regression pattern shows that the SEAS5 predictions are able to predict a pattern of Euro-Atlantic circulation anomalies connected to SAJET variability in early winter (Fig. 10) similar to the reanalysis (Fig. 9b), which also resembles to that of Figs. 4c and 7c over the North Atlantic region.

Using Eq. (2), the ENSO influence was removed from the SAJETI and then the reanalysis 200-hPa geopotential height anomalies were regressed onto the corresponding SAJETI residual (i.e., SAJETI linearly removed Niño-3.4) during early winter (Fig. 9c). A similar response of 200-hPa geopotential height anomalies is noted over the Euro-Atlantic region (Fig. 9c) compared to the reanalysis (Fig. 9b). The correlation between TWEIO and SAJETI residual is 0.35 (statistically significant at 95% confidence level), which is relatively weaker than that of total SAJETI and TWEIO. However, still it shows that pure SAJET can be modified substantially by the TWEIO precipitation dipole. Moreover, during early winter, the correlation of the SAJETI residual (independent of Niño-3.4 influence) with NAO index is 0.33 (statistically significant at 95% confidence level), which is almost similar to that of total SAJETI with NAO index (0.31). It means that SAJETI explains only about 10% of the total NAO variance. This is consistent with the NAO being an atmospheric mode that is mainly driven through the internal atmospheric dynamics (Jiménez-Esteve and Domeisen 2018). These results are consistent with Bader and Latif (2005), who argued that the decadal warming in the western TIO strongly impacts the NAO through a hemispheric wave pattern connected with the subtropical South Asian jet during the boreal winter (DJF) season. However, we note that this influence dominates in early compared to late winter.

To further investigate the mechanism connecting TIO precipitation dipole with North Atlantic variability, numerical

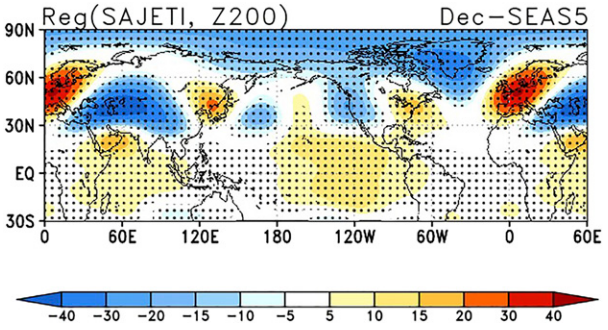

FIG. 10. Regression of ECMWF-SEAS5 200-hPa geopotential height anomalies (m) onto the corresponding SAJETI. Stippling denotes statistical significance at the 95% confidence level.

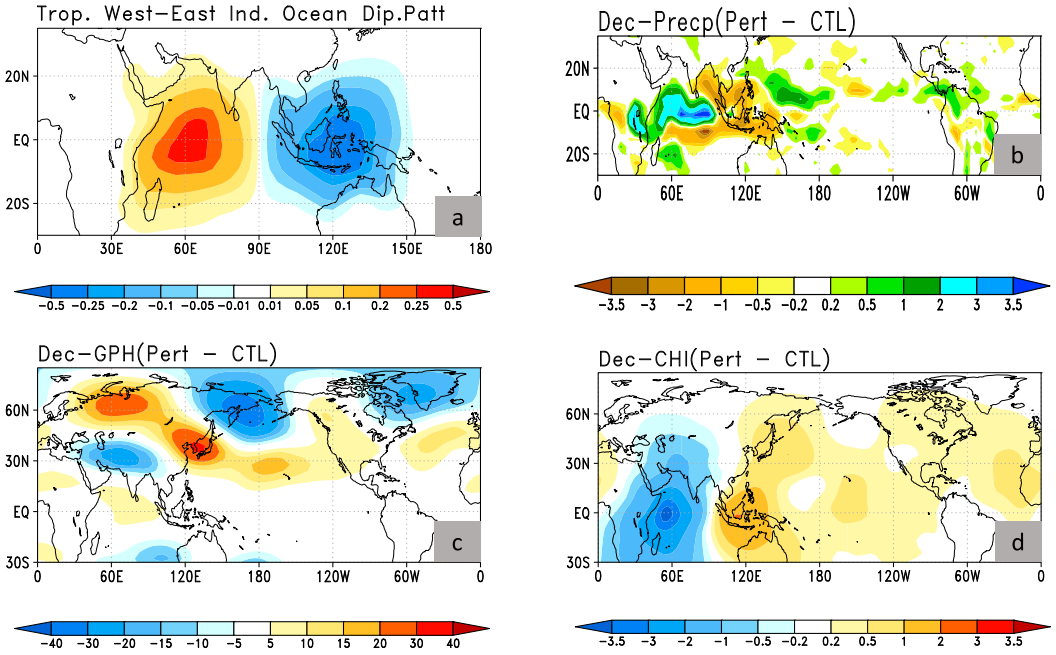

FIG. 11. (a) Tropical western (heating) and eastern (cooling) Indian Ocean (TWEIO) pattern for the idealized simulations (K day^{-1}). (b) Precipitation (Pert − CTL) response to the dipole (western warm/eastern cold) heating anomalies shown in (a) (mm day^{-1}) based on 139 ensemble members. (c) As in (b), but for 200-hPa geopotential height anomalies (m). (d) As in (c), but for 200-hPa velocity potential anomalies ($\times 10^6$ m^2 s^{-1}).

experiments have been carried out using the ICTP-AGCM, which are discussed in the next section.

d. Numerical experiments with idealized tropical forcing

Even though the statistical analyses described in the previous sections consistently suggest that forcing originated in the Indian Ocean produces an atmospheric response that propagates into the North Atlantic region, correlations or regressions (with no time lag) cannot be taken as a proof of causality. To demonstrate that the North Atlantic response originates from the Indian Ocean, we have performed numerical simulations with the ICTP atmospheric GCM (see section 2) in which we introduce diabatic heating perturbations to modify the precipitation distribution over the Indian Ocean.

Two experiments are carried out: one is the control (CTL) experiment with climatological boundary conditions and prescribed SSTs with no additional perturbation, and the other one is a perturbed (PERT) experiment adapted from Kosovelj et al. (2019) and Abid et al. (2020). In the PERT experiment, a dipole pattern of heating and cooling anomalies is added to the temperature tendency equation; the heating perturbation, located only in the tropical western and eastern Indian Ocean (Fig. 11a), is described in Eq. (3):

$$\left(\frac{\partial T}{\partial t}\right)_{\text{pert}}(\lambda,\varphi,\sigma) = F_{\text{SST}}(\lambda,\varphi)H_{\text{pert}}(\lambda,\varphi)\left(\frac{\partial T}{\partial t}\right)_{\text{cc}}(\varphi,\sigma). \quad (3)$$

In Eq. (3), the nondimensional factor F_{SST} (ranging from 0 to 1) defines the criterion to trigger the additional convective heating when SST meets the minimum threshold of 24°C, with values increasing linearly with SST above that limit. The spatial pattern of the perturbation is given by

$$H_{\text{pert}} = -k_h\cos(3\lambda)\text{rand}(0,1);\ \pi/6 < \lambda < 5\pi/6.$$

This term is finally multiplied by the zonally averaged temperature tendency produced by convection and large-scale condensation $(\partial T/\partial t)_{\text{cc}}$ to generate a three-dimensional heating perturbation.

The parameter $k_h = 0.5$ controls the heating amplitude in the perturbed experiment; the magnitude of k_h was chosen to trigger a convection dipole in the Indian Ocean comparable to that associated with a strong El Niño event, and is different from the value used by Kosovelj et al. (2019), where the larger value was chosen to mimic MJO variability with relatively small ensemble members. The positive or negative sign of the H_{pert} pattern corresponds to a heating or cooling term respectively; the pattern is multiplied at every day randomly with 0 or 1 at each grid point to simulate some high-frequency variability in the release of additional heating (or cooling). The heating and cooling dipole pattern is zonally confined in the tropical Indian ocean, with meridional extension of ±30° latitude (Kosovelj et al. 2019) as shown in Fig. 11a. For each experiment, the ICTP model was integrated for six months, starting from 1 October of different years, in order to create 139 ensemble members (Abid et al. 2020). Here, the response is analyzed for December only.

The precipitation anomaly simulated by the model as a response to the heating perturbation in the Indian Ocean is shown in Fig. 11b. As noted in Kosovelj et al. (2019), the dipole

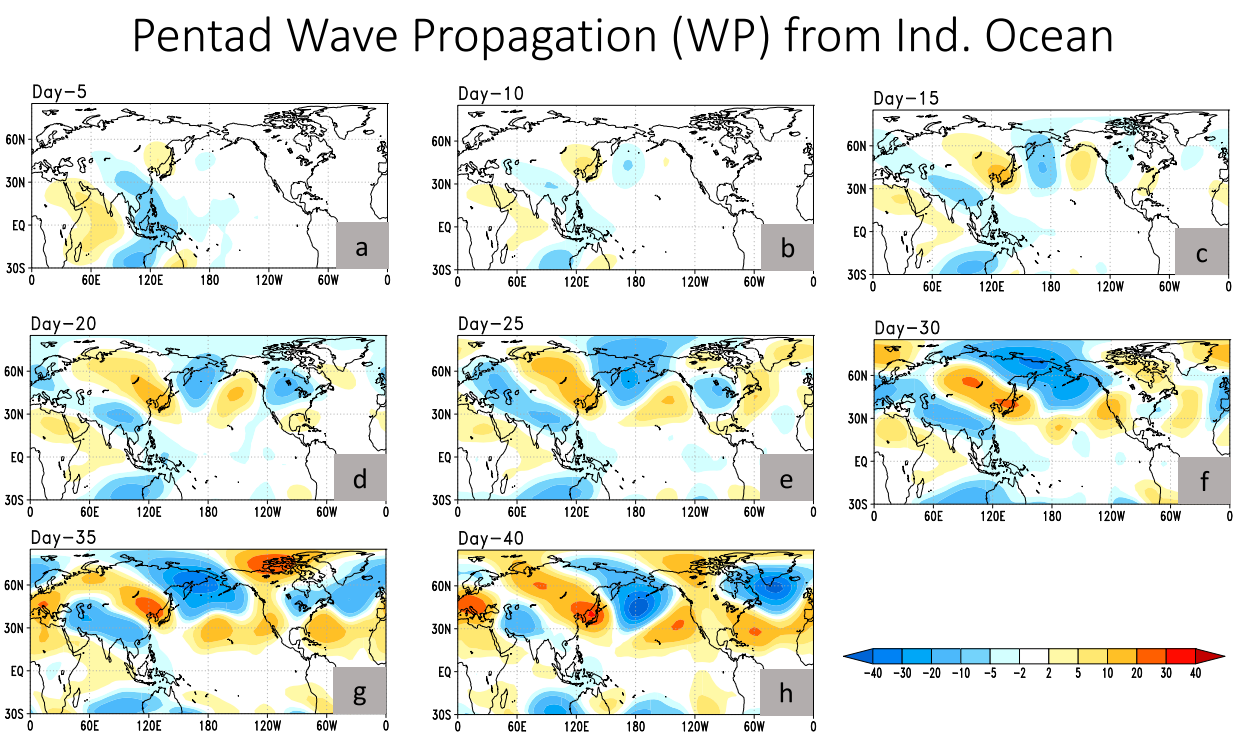

FIG. 12. (a)–(h) Ensemble-mean pentad (5-day mean) of the 200-hPa geopotential height (m) (Pert − CTL) representing the wave propagation due to the TWEIO heating anomalies in the Indian Ocean starting from 1 November. For days 1–5 the amplitude of the wave is ×5, because of its weaker amplitude. All others are on same scale.

perturbation produces a change in the precipitation pattern such that the total heating and cooling anomaly is amplified with respect to the imposed perturbation. The subtropical Rossby wave response over South Asia creates an upper-level trough over the western and central part of South Asia (Abid et al. 2020), which in turn modulates the subtropical SAJET. From this subtropical trough, a wavenumber-3 pattern propagates into the northern extratropics, leading to negative geopotential height anomalies over the Arctic and the Euro-Atlantic region (Fig. 11c). The 200-hPa velocity potential response reflects upper-level divergence anomalies over the western TIO and upper-level convergence anomalies over the eastern TIO (Fig. 11d). To the west of the upper-level anomalous convergence a streamfunction minimum appears due to Sverdrup balance (e.g., Rodwell and Hoskins 2001), leading to the negative geopotential height perturbation over South Asia and the associated perturbation of the subtropical South Asian jet (Fig. 11c). Therefore, our experiments confirm that the subtropical SAJET is modulated by the anomalous heating and cooling in the tropical Indian Ocean, and these South Asian jet anomalies act as a ''bridge'' between the tropical heating in the Indian Ocean and the Euro-Atlantic circulation anomalies in early winter. Moreover, we also performed an experiment with reversed Indian Ocean heating anomaly. Reversing the pattern of the Indian Ocean heating anomaly shows a response over Euro-Atlantic sector with centers of reverses sign, but slightly shifted to the south, which projects weakly onto the negative NAO phase (figure not shown).

To analyze the wave propagation from its tropical source in the Indian Ocean toward the North Atlantic sector, additional (Control and Perturbed) experiments were carried out with daily output frequency. The simulations were initialized from 1 November with the heating dipole turned on in the perturbed experiment. The reason for switching on the heating perturbations in November was to follow the wave propagation in late autumn (early winter). The experiments have 139 ensemble members with a similar forcing pattern shown in Fig. 11a. Pentad ensemble means (Perturbed − Control) have been analyzed for the 200-hPa geopotential height anomalies starting from 1 November shown in Fig. 12 (e.g., day 5 means the average from days 1 to 5, and so on). The initial pentad ensemble mean shows a Gill-type response (Fig. 12a) over the Indian Ocean corresponding to the wave source in the region. Initially, the wave amplitude is weak, and therefore the response in the first pentad was multiplied with 5. As time evolves, the wave emanating from the tropical Indian Ocean heating source passes through the North Pacific (Fig. 12b), and then after 15 days reaches to the North American sector (Fig. 12c). The wave propagates farther eastward and reaches the North Atlantic region after about 20 to 25 days (Figs. 12d,e). This wave propagation resembles the circumglobal teleconnection (CGT) following the waveguide in the vicinity of the mean jet stream position in the extratropical region as noticed by Branstator (2002). Moreover, the wave development in the North Atlantic is not only because of the linear wave propagation; eddy–mean state interactions, which

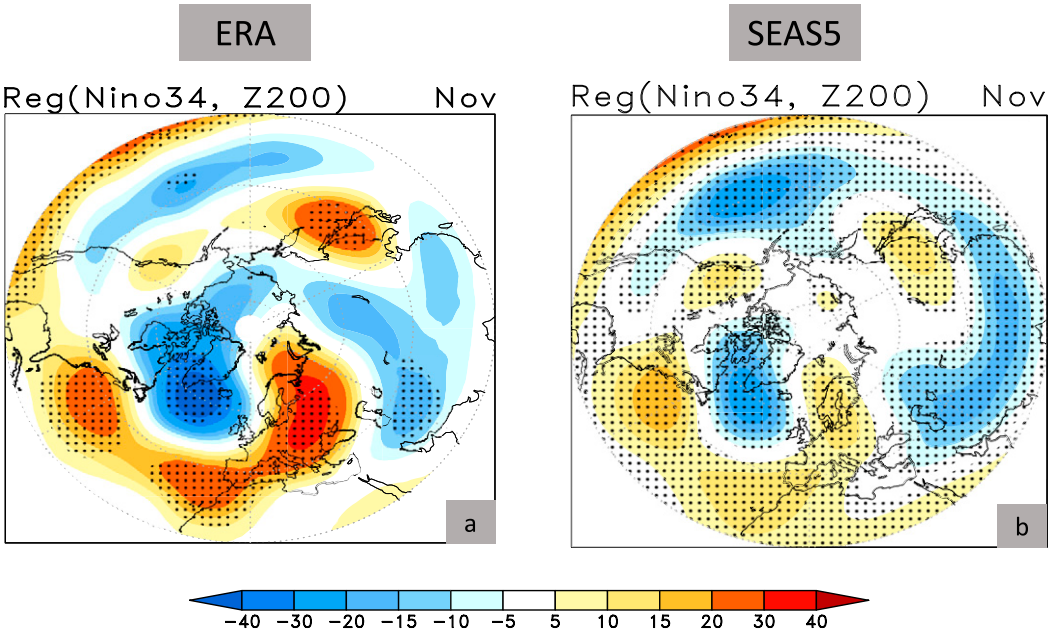

FIG. 13. (a),(b) Regression of reanalysis and the SEAS5 for the November 200-hPa geopotential height anomalies (m) onto their respective Niño-3.4 SST index for the period 1981–2015. Spatial correlation between the two patterns is 0.51. Stippling denotes statistical significance at the 95% confidence level.

dominate over that region, likely also play an important role (Jiménez-Esteve and Domeisen 2018). After 40 days, the upper-level (200-hPa) geopotential height anomalies response in the North Atlantic region is similar to that of Fig. 11c.

These well-simulated early winter teleconnections between the Indian Ocean and Euro-Atlantic sector with AGCM idealized numerical experiments compared to the reanalysis and the coupled model predictions (SEAS5) add robustness to our findings.

e. *Late-fall tropical teleconnections to the Euro-Atlantic circulation*

King et al. (2018a,b) have argued that the ENSO anomalies strongly modulate late fall (November) Euro-Atlantic circulation anomalies from central and central-eastern Pacific regions. Although the current study has focused on the Euro-Atlantic variability within the boreal winter (December–February) season, it is likely that the mechanism we investigated also works for the late fall circulation anomalies. The ENSO teleconnection to the Euro-Atlantic region in November (Fig. 13a) shows a similar spatial pattern but stronger in magnitude than its December counterpart (Fig. 1a), which is consistent with King et al. (2018b). In December, the NAO index over the Euro-Atlantic sector is 21.4 m, about 55% weaker than that of November (48.1 m; Fig. 13a). The ECMWF SEAS5 model reproduces the observed pattern over the Euro-Atlantic sector, but with weaker magnitude (Fig. 13b). Furthermore, separating the signals from the TWEIO and the Niño-3.4, we confirm that pure TWEIO enforces a positive and about 55% stronger NAO-like pattern over the Euro-Atlantic sector (Fig. 14b) in late fall, compared to the pure Niño-3.4 forcing (Fig. 14a).

4. Summary and conclusions

The present study focuses on the response of the Euro-Atlantic circulation anomalies to ENSO and its tropical interbasin connections across the boreal winter season. By separating early and late winter, it is noticed that the heating anomalies from the central-eastern equatorial Pacific (Niño-3.4 region) are the main source of teleconnections with the Euro-Atlantic circulation anomalies in late winter (February), whereas they play a lesser direct role in early winter (December). During early winter, the primary forcing that modulates the positive NAO-like response in the Euro-Atlantic region comes from a tropical western and eastern Indian Ocean dipole, namely as the tropical western–eastern Indian Ocean (TWEIO) dipole (e.g., see Figs. 4a and 6c). In this part of the season, a warm ENSO event is connected to a precipitation dipole in the tropical Indian Ocean, where heating anomalies are located in the tropical western Indian Ocean and cooling anomalies are in the eastern Indian Ocean. The correlation between observed TWEIO and Niño-3.4 in early winter (December) is 0.64, which explains about 40% of the TWEIO variability. It also implies that TWEIO can exist independently, with a periodicity of about 3 years.

Instead of using SST-based indices to compute teleconnections, we used precipitation indices from the Niño-3.4 region as well as a TWEIO dipole index from the tropical Indian Ocean. The correlation of the NAO with TWEIO is 0.38, while with Niño-3.4 it is 0.24, indicating a dominant role of the Indian Ocean in modulating Euro-Atlantic circulation anomalies in early winter. Importantly, it is noted that the precipitation forcing from the two oceanic basins can exist

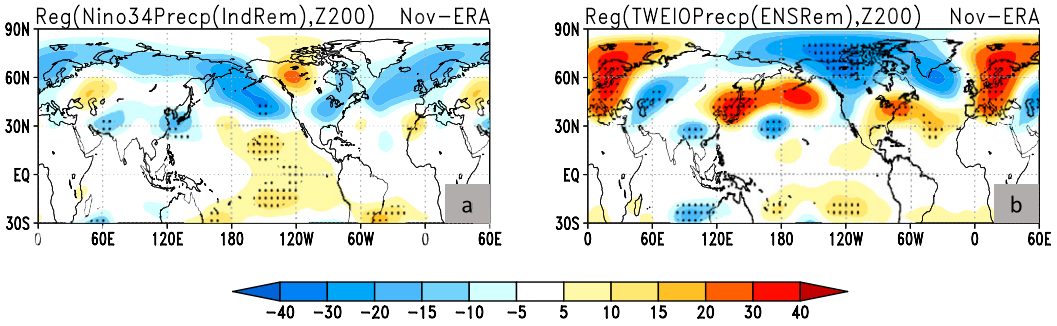

FIG. 14. (a) Regression of the reanalysis November 200-hPa geopotential height anomalies (m) onto the pure Niño-3.4 precipitation anomalies index (after removing TWEIO) for the period 1981–2015. (b) As in (a), but now with pure TWEIO precipitation index (after removing Niño-3.4). Stippling denotes statistical significance at the 95% confidence level.

independently from each other. During early winter (December), significant teleconnections with the Euro-Atlantic circulation anomalies are predominantly found with pure TWEIO heating anomalies forcing a positive NAO (Fig. 6c), while a stronger (~50%) impact of pure Niño-3.4 is seen over the Aleutian low in the PNA sector (Fig. 6a). However, in late winter (February), pure ENSO (Niño-3.4) dominates and favors negative NAO in the Euro-Atlantic region. We also noted an opposite response of AO anomalies to the Indian and Pacific Ocean forcings, where Indian Ocean dominates in modulating the positive AO like response during early, while ENSO favors a negative AO response in late winter.

The Indian Ocean teleconnection develops an upper-level (200-hPa) wavenumber-3 Rossby wave pattern originating from the subtropical South Asian jet (SAJET) region, which is modulated by the TWEIO dipole; this wave pattern shows a strong trough over the North Atlantic sector in early winter (December). The TWEIO dipole induces upper-level convergence in the eastern and divergence in the western Indian Ocean. This enforces an upper-level cyclonic circulation with a negative geopotential height anomaly over the subtropical South Asian region. From there, the wave train propagates to the northeast and eventually reaches the North Atlantic region, where it leads to a positive NAO-like response during early winter. Our results are consistent with Bader and Latif (2005), who found linkages between Indian Ocean SSTs and North Atlantic atmospheric circulation on decadal time scales during boreal winter (December–February). However, by separating early and late winter, we have shown that this physical mechanism is only active in early winter. The generation and propagation of Rossby waves from the subtropical South Asia to the North Atlantic has been confirmed with numerical AGCM experiments, where precipitation anomalies over the Indian Ocean were induced by an additional diabatic forcing shaped as a TWEIO heating and cooling dipole (Figs. 11 and 12).

Moreover, considering the results from King et al. (2018a)—who showed that late autumn to early winter warming in the European region is related to the negative geopotential height anomalies in the northern Atlantic and positive anomalies in the subtropical Atlantic (mimicking positive NAO)—our results imply that the European warming is mainly induced by the tropical Indian Ocean in late fall as well as in early winter. In conclusion, we argue that the ENSO interbasin teleconnection with the Indian Ocean is the main linkage between ENSO and the Euro-Atlantic circulation anomalies in early winter, although the Indian Ocean forcing can also be present independently of ENSO. The mechanisms for early and late winter teleconnections are summarized in the schematic shown in Fig. 15.

The ECMWF-SEAS5 predictions reproduce the transition from the Indian Ocean teleconnection in early winter to the

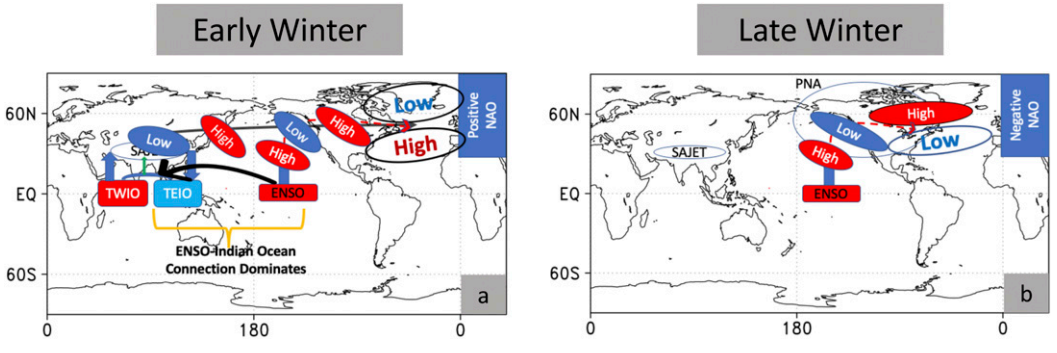

FIG. 15. Schematic illustration of the mechanism for the (a) early to (b) late winter transition of the Euro-Atlantic circulation anomalies and their possible tropospheric pathways.

direct ENSO teleconnection with the Euro-Atlantic circulation anomalies in late winter. SEAS5 simulates the Rossby wave originating from the subtropical SAJET region modulated by the Indian Ocean; however, the amplitude of the wave pattern over the northern extratropics including the North Atlantic sector is underestimated compared to that of reanalysis. These results have implications for the subseasonal to seasonal predictability of the Euro-Atlantic circulation anomalies, which will be analyzed in detail in future studies.

We argue that a subseasonal analysis is required for the detailed understanding of the large-scale variability and predictability of the regional circulation anomalies, even at interannual time scales. Consistently with earlier studies (e.g., King et al. 2018a; Ayarzagüena et al. 2018; Scaife et al. 2017), we found that instead of averaging over a 3-month (DJF) season, separating into early and late winter leads to a more appropriate assessment of the intraseasonal variability of the Euro-Atlantic circulation anomalies. Finally, the main results about the role of the Indian Ocean, found in this study with reanalysis and the ECMWF-SEAS5 reforecasts, could be investigated further using a multimodel dataset. Extending our analysis to historical multidecadal simulations may be beneficial for attribution studies linking the recent warming trends in the Indian Ocean to extreme circulation anomalies over the Euro-Atlantic region.

Acknowledgments. The lead author would like to acknowledge the Earth System Physics Section of ICTP and the Centre of Excellence for Climate Change Research (CECCR) for their support. The lead author also like to thank the King Abdulaziz University High Performance Centre (https://hpc.kau.edu.sa). The authors thank Dr. Martin P. King for his valuable comments and suggestions. We also like to thank the three anonymous reviewers and editors for their insightful comments that have indeed improved the manuscript.

Data availability statement. The seasonal hindcast datasets were provided by the Copernicus Climate Change Service through its ECMWF portal (https://climate.copernicus.eu), while the ECMWF reanalysis datasets were obtained from https://apps.ecmwf.int/. The SPEEDY AGCM is available from https://www.ictp.it/research/esp/models/speedy.aspx, and experiment data will be available on request.

REFERENCES

Abid, M. A., I.-S. Kang, M. Almazroui, and F. Kucharski, 2015: Contribution of synoptic transients to the potential predictability of PNA circulation anomalies: El Niño vs La Niña. *J. Climate*, **28**, 8347–8362, https://doi.org/10.1175/JCLI-D-14-00497.1.

——, M. Ashfaq, F. Kucharski, K. J. Evans, and M. Almazroui, 2020: Tropical Indian Ocean mediates ENSO influence over Central Southwest Asia during the wet season. *Geophys. Res. Lett.*, **47**, e2020GL089308, https://doi.org/10.1029/2020GL089308.

Adler, R. F., and Coauthors, 2003: The version 2 Global Precipitation Climatology Project (GPCP) monthly precipitation analysis (1979–present). *J. Hydrometeor.*, **4**, 1147–1167, https://doi.org/10.1175/1525-7541(2003)004<1147:TVGPCP>2.0.CO;2.

Annamalai, H., H. Okajima, and M. Watanabe, 2007: Possible impact of the Indian Ocean SST on the Northern Hemisphere circulation during El Niño. *J. Climate*, **20**, 3164–3189, https://doi.org/10.1175/JCLI4156.1.

Ayarzagüena, B., S. Ineson, N. J. Dunstone, M. P. Baldwin, and A. A. Scaife, 2018: Intraseasonal effects of El Niño–Southern Oscillation on North Atlantic climate. *J. Climate*, **31**, 8861–8873, https://doi.org/10.1175/JCLI-D-18-0097.1.

——, J. López-Parages, M. Iza, N. Calvo, and B. Rodríguez-Fonseca, 2019: Stratospheric role in interdecadal changes of El Niño impacts over Europe. *Climate Dyn.*, **52**, 1173–1186, https://doi.org/10.1007/s00382-018-4186-3.

Bader, J., and M. Latif, 2005: North Atlantic Oscillation response to anomalous Indian Ocean SST in a coupled GCM. *J. Climate*, **18**, 5382–5389, https://doi.org/10.1175/JCLI3577.1.

Berrisford, P., and Coauthors, 2011: The ERA-Interim Archive: Version 2.0. ERA Rep. Series 1, 23 pp., https://www.ecmwf.int/en/elibrary/8174-era-interim-archive-version-20.pdf.

Bladé, I., M. Newman, M. A. Alexander, and J. D. Scott, 2008: The late fall extratropical response to ENSO: Sensitivity to coupling and convection in the tropical west Pacific. *J. Climate*, **21**, 6101–6118, https://doi.org/10.1175/2008JCLI1612.1.

Branstator, G., 2002: Circumglobal teleconnections, the jet stream waveguide, and the North Atlantic Oscillation. *J. Climate*, **15**, 1893–1910, https://doi.org/10.1175/1520-0442(2002)015<1893:CTTJSW>2.0.CO;2.

Brönnimann, S., 2007: Impact of El Niño–Southern Oscillation on European climate. *Rev. Geophys.*, **45**, RG3003, https://doi.org/10.1029/2006RG000199.

Butler, A. H., L. M. Polvani, and C. Deser, 2014: Separating the stratospheric and tropospheric pathways of El Niño–Southern Oscillation teleconnections. *Environ. Res. Lett.*, **9**, 024014, https://doi.org/10.1088/1748-9326/9/2/024014.

Cai, W. J., P. van Rensch, T. Cowan, and H. H. Hendon, 2011: Teleconnection pathways of ENSO and the IOD and mechanism for impacts on Australian rainfall. *J. Climate*, **24**, 3910–3923, https://doi.org/10.1175/2011JCLI4129.1.

——, and Coauthors, 2019: Pantropical climate interactions. *Science*, **363**, eaav4236, https://doi.org/10.1126/science.aav4236.

Dee, D. P., and Coauthors, 2011: The ERA-Interim reanalysis: Configuration and performance of the data assimilation system. *Quart. J. Roy. Meteor. Soc.*, **137**, 553–597, https://doi.org/10.1002/qj.828.

Deser, C., I. R. Simpson, A. S. Phillips, and K. A. McKinnon, 2018: How well do we know ENSO's climate impacts over North America, and how do we evaluate models accordingly? *J. Climate*, **31**, 4991–5014, https://doi.org/10.1175/JCLI-D-17-0783.1.

Domeisen, D. I. V., A. H. Butler, K. Fröhlich, M. Bittner, W. A. Müller, and J. Baehr, 2015: Seasonal predictability over Europe arising from El Niño and stratospheric variability in the MPI-ESM seasonal prediction system. *J. Climate*, **28**, 256–271, https://doi.org/10.1175/JCLI-D-14-00207.1.

——, C. I. Garfinkel, and A. H. Butler, 2019: The teleconnection of El Niño Southern Oscillation to the stratosphere. *Rev. Geophys.*, **57**, 5–47, https://doi.org/10.1029/2018RG000596.

Feudale, L., and F. Kucharski, 2013: A common mode of variability of African and Indian monsoon rainfall at decadal timescale. *Climate Dyn.*, **41**, 243–254, https://doi.org/10.1007/s00382-013-1827-4.

Fletcher, C. G., and P. J. Kushner, 2011: The role of linear interference in the annular mode response to tropical SST forcing. *J. Climate*, **24**, 778–794, https://doi.org/10.1175/2010JCLI3735.1.

——, and C. Cassou, 2015: The dynamical influence of separate teleconnections from the Pacific and Indian Oceans on the

northern annular mode. *J. Climate*, **28**, 7985–8002, https://doi.org/10.1175/JCLI-D-14-00839.1.

García-Serrano, J., B. Rodríguez-Fonseca, I. Bladé, P. Zurita-Gotor, and A. de la Cámara, 2011: Rotational atmospheric circulation during North Atlantic–European winter: The influence of ENSO. *Climate Dyn.*, **37**, 1727–1743, https://doi.org/10.1007/s00382-010-0968-y.

Hardiman, S. C., N. J. Dunstone, A. A. Scaife, D. M. Smith, S. Inseon, J. Lim, and D. Fereday, 2019: The impact of strong El Niño and La Niña events on the North Atlantic. *Geophys. Res. Lett.*, **46**, 2874–2883, https://doi.org/10.1029/2018GL081776.

Herceg-Bulić, I., C. Brankovic, and F. Kucharski, 2012: Winter ENSO teleconnections in a warmer climate. *Climate Dyn.*, **38**, 1593–1613, https://doi.org/10.1007/s00382-010-0987-8.

Hitchcock, P., and I. R. Simpson, 2014: The downward influence of stratospheric sudden warmings. *J. Atmos. Sci.*, **71**, 3856–3876, https://doi.org/10.1175/JAS-D-14-0012.1.

Honda, M., J. Inoue, and S. Yamane, 2009: Influence of low Arctic sea-ice minima on anomalously cold Eurasian winters. *Geophys. Res. Lett.*, **36**, L08707, https://doi.org/10.1029/2008GL037079.

Hoskins, B., and D. Karoly, 1981: The steady linear response of a spherical atmosphere to thermal and orographic forcing. *J. Atmos. Sci.*, **38**, 1179–1196, https://doi.org/10.1175/1520-0469(1981)038<1179:TSLROA>2.0.CO;2.

Ineson, S., and A. A. Scaife, 2009: The role of the stratosphere in the European climate response to El Niño. *Nat. Geosci.*, **2**, 32–36, https://doi.org/10.1038/ngeo381.

Jiménez-Esteve, B., and D. I. V. Domeisen, 2018: The tropospheric pathway of the ENSO–North Atlantic teleconnection. *J. Climate*, **31**, 4563–4584, https://doi.org/10.1175/JCLI-D-17-0716.1.

Johnson, S. J., and Coauthors, 2019: SEAS5: The new ECMWF seasonal forecast system. *Geosci. Model Dev. Discuss.*, **12**, 1087–1117, https://doi.org/10.5194/gmd-12-1087-2019.

King, M. P., I. Herceg-Bulić, I. Bladé, J. García-Serrano, N. Keenlyside, F. Kucharski, C. Li, and S. Sobolowski, 2018a: Importance of late fall ENSO teleconnection in the Euro-Atlantic sector. *Bull. Amer. Meteor. Soc.*, **99**, 1337–1343, https://doi.org/10.1175/BAMS-D-17-0020.1.

——, ——, F. Kucharski, and N. Keenlyside, 2018b: Interannual tropical Pacific sea surface temperature anomalies teleconnection to Northern Hemisphere atmosphere in November. *Climate Dyn.*, **50**, 1881–1899, https://doi.org/10.1007/s00382-017-3727-5.

Kosovelj, K., F. Kucharski, F. Molteni, and N. Zagar, 2019: Modal decomposition of the global response to tropical heating perturbations resembling MJO. *J. Atmos. Sci.*, **76**, 1457–1469, https://doi.org/10.1175/JAS-D-18-0203.1.

Kucharski, F., F. Molteni, and A. Bracco, 2006: Decadal interactions between the western tropical Pacific and the North Atlantic Oscillation. *Climate Dyn.*, **26**, 79–91, https://doi.org/10.1007/s00382-005-0085-5.

——, A. Bracco, J. H. Yoo, A. M. Tompkins, L. Feudale, P. Ruti, and A. Dell'Aquila, 2009: A Gill–Matsuno-type mechanism explains the tropical Atlantic influence on African and Indian monsoon rainfall. *Quart. J. Roy. Meteor. Soc.*, **135**, 569–579, https://doi.org/10.1002/qj.406.

——, F. Molteni, M. P. King, R. Farneti, I.-S. Kang, and L. Feudale, 2013: On the need of intermediate complexity general circulation models: A "SPEEDY" example. *Bull. Amer. Meteor. Soc.*, **94**, 25–30, https://doi.org/10.1175/BAMS-D-11-00238.1.

Kumar, A., M. Chen, and W. Wang, 2013: Understanding prediction skill of seasonal mean precipitation over the tropics. *J. Climate*, **26**, 5674–5681, https://doi.org/10.1175/JCLI-D-12-00731.1.

Lee, R. W., S. J. Woolnough, A. J. Charlton-Perez, and F. Vitart, 2019: ENSO modulation of MJO teleconnections to the North Atlantic and Europe. *Geophys. Res. Lett.*, **46**, 13 535–13 545, https://doi.org/10.1029/2019GL084683.

McIntosh, P. C., and H. H. Hendon, 2018: Understanding Rossby wave trains forced by the Indian Ocean dipole. *Climate Dyn.*, **50**, 2783–2798, https://doi.org/10.1007/s00382-017-3771-1.

Mezzina, B., J. Garcia-Serrano, I. Bladé, and F. Kucharski, 2019: Dynamics of the ENSO teleconnection and NAO variability in the North Atlantic-European late winter. *J. Climate*, **33**, 907–923, https://doi.org/10.1175/JCLI-D-19-0192.1.

Molteni, F., 2003: Atmospheric simulations using a GCM with simplified physical parametrizations. I: Model climatology and variability in multi-decadal experiments. *Climate Dyn.*, **20**, 175–191, https://doi.org/10.1007/s00382-002-0268-2.

——, T. N. Stockdale, and F. Vitart, 2015: Understanding and modelling extratropical teleconnections with the Indo-Pacific region during the northern winter. *Climate Dyn.*, **45**, 3119–3140, https://doi.org/10.1007/s00382-015-2528-y.

——, and Coauthors, 2020: Boreal-winter teleconnections with tropical Indo-Pacific rainfall in HighResMIP historical simulations from the PRIMAVERA project. *Climate Dyn.*, **55**, 1843–1873, https://doi.org/10.1007/s00382-020-05358-4.

Moron, V., and I. Gouirand, 2003: Seasonal modulation of the El Niño–Southern Oscillation relationship with sea level pressure anomalies over the North Atlantic in October–March 1873–1996. *Int. J. Climatol.*, **23**, 143–155, https://doi.org/10.1002/joc.868.

Rayner, N. A., D. E. Parker, E. B. Horton, C. K. Folland, L. V. Alexander, D. P. Rowell, E. C. Kent, and A. Kaplan, 2003: Global analyses of sea surface temperature, sea ice, and night marine air temperature since the late nineteenth century. *J. Geophys. Res.*, **108**, 4407, https://doi.org/10.1029/2002JD002670.

Rodwell, M. J., and B. J. Hoskins, 2001: Subtropical anticyclones and summer monsoons. *J. Climate*, **14**, 3192–3211, https://doi.org/10.1175/1520-0442(2001)014<3192:SAASM>2.0.CO;2.

Ruggieri, P., F. Kucharski, R. Buizza, and M. H. P. Ambaum, 2017: The transient atmospheric response to a reduction of sea-ice cover in the Barents and Kara Seas. *Quart. J. Roy. Meteor. Soc.*, **143**, 1632–1640, https://doi.org/10.1002/qj.3034.

Saji, N. H., B. N. Goswami, P. N. Vinayachandran, and T. Yamagata, 1999: A dipole mode in the tropical Indian Ocean. *Nature*, **401**, 360–363, https://doi.org/10.1038/43854.

Sardeshmukh, P. D., and B. J. Hoskins, 1988: The generation of global rotational floe by steady idealized tropical divergence. *J. Atmos. Sci.*, **45**, 1228–1251, https://doi.org/10.1175/1520-0469(1988)045<1228:TGOGRF>2.0.CO;2.

Scaife, A. A., and Coauthors, 2017: Tropical rainfall, Rossby waves and regional winter climate predictions. *Quart. J. Roy. Meteor. Soc.*, **143**, 1–11, https://doi.org/10.1002/qj.2910.

Shimizu, M. H., and I. F. de Albuquerque Cavalcanti, 2011: Variability patterns of Rossby wave source. *Climate Dyn.*, **37**, 441–454, https://doi.org/10.1007/s00382-010-0841-z.

Shinoda, T., M. A. Alexander, and H. H. Hendon, 2004: Remote response of the Indian Ocean to interannual SST variations in tropical Pacific. *J. Climate*, **17**, 362–372, https://doi.org/10.1175/1520-0442(2004)017<0362:RROTIO>2.0.CO;2.

Sigmond, M., J. F. Scinocca, V. V. Kharin, and T. G. Shepherd, 2013: Enhanced seasonal forecast skill following stratospheric

sudden warmings. *Nat. Geosci.*, **6**, 98–102, https://doi.org/10.1038/ngeo1698.

Takaya, K., and H. Nakamura, 2001: A formulation of a phase-independent wave-activity flux for stationary and migratory quasigeostrophic eddies on a zonally varying basic flow. *J. Atmos. Sci.*, **58**, 608–627, https://doi.org/10.1175/1520-0469(2001)058<0608:AFOAPI>2.0.CO;2.

Thompson, D. W. J., and J. M. Wallace, 2000: Annular modes in the extratropical circulation. Part I: Month-to-month variability. *J. Climate*, **13**, 1000–1016, https://doi.org/10.1175/1520-0442(2000)013<1000:AMITEC>2.0.CO;2.

Toniazzo, T., and A. A. Scaife, 2006: The influence of ENSO on winter North Atlantic climate. *Geophys. Res. Lett.*, **33**, L24704, https://doi.org/10.1029/2006GL027881.

Trascasa-Castro, P., A. C. Maycock, Y. Y. S. Yiu, and J. K. Fletcher, 2019: On the linearity of the stratospheric and Euro-Atlantic sector response to ENSO. *J. Climate*, **32**, 6607–6626, https://doi.org/10.1175/JCLI-D-18-0746.1.

Wang, C., 2019: Three-ocean interactions and climate variability: A review and perspective. *Climate Dyn.*, **53**, 5119–5136, https://doi.org/10.1007/s00382-019-04930-x.

Yu, B., and H. Lin, 2016: Tropical atmospheric forcing of the wintertime North Atlantic Oscillation. *J. Climate*, **29**, 1755–1772, https://doi.org/10.1175/JCLI-D-15-0583.1.

Zhong, A., H. H. Hendon, and O. Alves, 2005: Indian Ocean variability and its association with ENSO in a global coupled model. *J. Climate*, **18**, 3634–3649, https://doi.org/10.1175/JCLI3493.1.